On the Performance of IEEE 802.11n: Analytical and Simulations Results

André Michelin Câmara and Roger Pierre Fabris Hoefel

***Abstract*—This paper shows analytical and simulation results on the performance of IEEE 802.11 physical (PHY) layer over additive white Gaussian noise (AWGN) and TGn channel models.**

***Keywords*—802.11n, MIMO, TGn channel models.**

Resumo—Neste artigo utiliza-se técnicas analíticas e computacionais para investigar o desempenho da camada física do sistema IEEE 802.11n em canais AWGN e TGn.

Palavras-chave—802.11n, MIMO, modelos de canal TGn.

I. Introduction

The 802.11n amendment to the wireless local area network (WLAN) IEEE 802.11 standard was released in its final version in late 2009 [1]. It supports data rates up to *600 Mbps* and it is legacy compatible with IEEE 802.11g and 802.11a amendments, which share the same Industrial, Scientific and Medical (ISM) band at *2.4 GHz* and *5.8 GHz*, respectively. To achieve extremely high data rates over wireless channels, the 802.11n standard uses state of art PHY layer digital communication techniques and medium access control (MAC) layer protocols. The PHY layer is based on orthogonal frequency-division multiplexing (OFDM), using channels with bandwidth of *20 MHz* and *40 MHz*. The PHY layer is also founded on the multiple input multiple output (MIMO) paradigm, using multiple antennas perform transmit beamforming; receive beamforming and spatial division multiplexing (SDM).

As far we are concerned many of the performance results and details of the optimized algorithms used in 802.11n chip sets are industrial valuable knowledge. Therefore, this paper aims to show analytical and simulation results that can be used as a basic framework to analyze the system performance in diverse and harsh environments, clearly identifying which aspects must be improved and optimized. To accomplish our targets, this paper is organized as follows. Section II describes the 802.11n standard and the simulator architecture that we have been developing. Section III develops fundamental aspects on the mathematical and computational modeling, making possible to other researches to reproduce the obtained results (i.e., a fundamental issue for the scientific community). A through comparison between numerical and simulation results is carried out in Section IV. Finally, Section V presents our final remarks.

II. IEEE 802.11n and Simulator Architecture

This section contains the underlying information to the remaining of this paper, describing jointly the IEEE 802.11n standard and the architecture of an IEEE 802.11n simulator that we have been developing.

André Michelin Câmara, Delet, UFRGS, Porto Alegre, RS, Brazil. E-mail: andre.camara@ufrgs.br.

Roger Pierre Fabris Hoefel, Department of Electrical Enginnering, Federal University of Rio Grande do Sul (UFRGS), Porto Alegre, Rio Grande do Sul (RS), Brazil; E-mail: roger.hoefel@ufrgs.br.

The 802.11n standard defines two basic packet formats, called high throughput (HT) modes [1, p.258]. The first format, the HT mixed format (MF) packet, is divided in two parts: *(1)* the first one is legacy compatible with devices that implement the 802.11a/g amendments; *(2)* the second one contains the HT fields. The MF mode is mandatory for 802.11n devices. The second format is the optional HT Greenfield (GF), which is a pure HT packet and has no legacy compatibility. This paper focuses only on the HT-MF packet operating at 20 MHz bandwidth due to space constraints.

A. HT-MF Packet

The HT-MF packet is shown in Fig. 1. The legacy preamble contains the legacy short training field (L-STF), the legacy long training field (L-LTF) and the legacy signal field (L-SIG). The first one carries ten repetitions of a short symbol, used to packet detection, automatic gain control (AGC) and gross time and frequency synchronization. The L-LTF contains two long symbols plus the cyclic prefix (CP). These symbols are used for channel estimation and fine time and frequency synchronization. The next field contains a control symbol, which transports control information about the transmitted packet in the legacy format, called legacy signal field (L-SIG). This symbol must be correctly decoded by the legacy devices to avoid interfering in the ongoing atomic cycle. If a legacy receiver does not decode this symbol correctly, it must rely on a power detection scheme to identify when the channel is busy. In the legacy preamble, the same signal is transmitted in all transmitting antennas. Hence, it is necessary to decorrelate the signal in order to mitigate undesirable beamforming effects. To accomplish this, a different cyclic shift (CS) is applied at each antenna. The next field is the HT-SIG field, which has two control OFDM symbols with CP. It contains essential information about the packet, as the payload length, modulation coding scheme (MCS) and so forth.

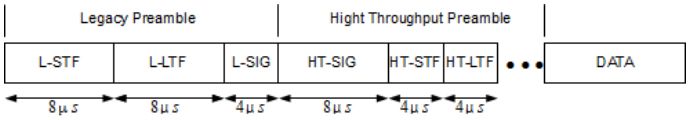

Fig. 1. HT-MF packet structure.

The CSs used in the legacy portion are smaller than the CSs applied in rest of the packet, once a larger CS in the legacy preamble would degrade the legacy compatibility [2]. Hence, the following HT fields use larger CSs, optimized to the correct operation of the AGC, refined using the HT-STF, and MIMO channel estimation (carried out using the HT-LTF symbols). The number of HT-LTF symbols depends on the number of spatial streams transmitted [1, p. 280]. Finally, the data field contains an OFDM symbol resultant from the inverse discrete Fourier transform (IDFT) of the orthogonal subcarriers that transport the information data and pilot symbols plus a cyclic CP. The CP is added to make the system robust against inter-symbol interference (ISI) and inter-carrier interference (ICI).

B. TRANSMITTER ARCHITECTURE

The transmitter model developed in our simulator follows the 802.11n standard *ipsis litteris* in its essential structure [1], only eliminating signal processing operations that are not essential for a baseband discrete time simulation, as the digital-to-analog conversion (DAC) and analog radio frequency (RF) processing.

The PHY layer receives from the MAC layer the bits to be transmitted and the *TXVECTOR*, which contains control information about the packet (e.g., packet length, channel bandwidth, CP length, MCS) [1, p. 249-255]. The MCS mode defines the number of spatial streams (N_{SS}), modulation and code rate (R) for the packet. The MCS is numbered from 0 to 76, where the modes ranging from 0 to 31 use equal modulation (EQM) on all streams. These modes are divided as follows: *(i)* 0 to 7 have a single spatial stream; *(ii)* 8 to 15 have two spatial streams; *(iii)* 16 to 23 have three spatial streams; *(iv)* 24 to 31 have four spatial streams. MCS 33 to 76 define unequal modulation on each stream. Tab. I shows the MCS parameters for the modes 0 to 31, where N_{BPSCS} is the number of bits per subcarrier per stream (i.e., the modulation cardinality).

TABLE I - MODULATION AND CODE SCHEMES.

Modulation, Code Rate	N_{BPSCS}	MCS			
		N_{SS} 1	N_{SS} 2	N_{SS} 3	N_{SS} 4
BPSK, R=1/2	1	0	8	16	24
QPSK, R=1/2	2	1	9	17	25
QPSK, R=3/4	2	2	10	18	26
16-QAM, R=1/2	4	3	11	19	27
16-QAM, R=3/4	4	4	12	20	28
64-QAM, R=2/3	6	5	13	21	29
64-QAM, R=3/4	6	6	14	22	30
64-QAM, R=5/6	6	7	15	23	31

The packet information, obtained from the TXVECTOR, together with the MAC protocol data unit (PDU) are enough to generate the entire PHY packet. Regarding the data symbols, the first step is to create the *Data field*, which consists of: 16-bits Service Field; information bits; six tail bits and padding bits [1, p. 287]. In the next step, the bits from the data field are scrambled using the same scrambler defined in the 802.11a amendment [3 p. 16]. The scrambler output bits are processed by the forward error correcting (FEC) encoder, which has two flavors: binary convolutional code (BCC) or low-density parity-check (LDPC) code. The base code rate for the BCC is ½. The BBC output is punctured to form codes with rates of 2/3, 3/4 and 5/6. After this, the encoded bits are sent to the parser, which is responsible for the separation of the coded bits into spatial streams. In the next step, the bits are divided into symbols. The interleaving is applied to the coded bits for each OFDM symbol [4, p.86]. In the following, the bits are mapped in constellation points, resulting in complex data symbols transported at each OFDM subcarrier. Pilots are inserted and then each OFDM symbol is converted to time domain using the inverse Fast Fourier Transform (IFFT). Next, the CS is applied in each symbol at each transmitting antenna. The CP is added using the final samples of each OFDM symbol. The preamble is put in front of the data field, creating a complete HT-MF packet.

C. RECEIVER ARCHITECTURE

The receiver structure is not defined in the 802.11n amendment. Fig. 3 depicts the receiver architecture used in this paper, structured to receive only HT-MF packets

The first block is the packet detector, which uses the L-STF to detect the arriving of a packet. After packet detection, it is necessary to obtain the time synchronization, i.e., to estimate the position of the OFDM symbols inside the packet. The time synchronization is performed using the L-STF and L-LTF symbols. The frequency offset, estimated using these same fields, is used to correct the remaining fields of the MF-HT packet. It is implemented a time domain autocorrelation algorithm to detect the packet, synchronize the OFDM symbols and to estimate the frequency offset [2].

The next step is to perform the FFT of the L-LTF to estimate the channel. However, this procedure does not allow estimating a MIMO channel, therefore, this first channel estimation is used only to detect the L-SIG and HT-SIG fields, which are single streams ones. The procedure to obtain the control information in the L-SIG and HT-SIG symbols is the same used for the data symbols, except that the scrambler is not performed in the SIG fields. Note that the both L-SIG and HT-SIG fields are convolutional coded with rate ½, interleaved, and then modulated using binary phase-shift keying (BPSK).

The procedure to receive the data symbols is implemented as follows. First, the CP is removed, remaining only the 64 time samples of each OFDM symbol. These samples are used to perform the 64-point FFT for each OFDM symbol. The MIMO channel estimation is implemented in the frequency domain using the HT-LTFs [4, p. 94]. The subcarriers are equalized using this MIMO channel estimation. Two equalizer algorithms have been implemented: zero-forcing (ZF) [4, p. 33, 96] and minimum mean square error (MMSE) [4, p. 47]. The four pilot symbols transmitted at each OFDM data symbol are used to estimate and correct the residual phase due to the imperfect time and frequency synchronization. The block called demapper performs hard or soft demodulation of the data symbols transport by the OFDM subcarriers. In the case of soft demodulation, the metrics are calculated using the methodology proposed in [5]. The de-interleaving e deparser reverse the corresponding operations performed at the transmitter side. Next, it is implement the Viterbi decoding, using soft or hard decoding. Finally, the decoded bits go into the descrambler to recover the streams of transmitted bits.

III – ANALYTICAL RESULTS AND SIMULATION MODELING

The IEEE 802.11n and 802.11a/g PHY layer simulator has been developed using *Matlab* and *C*++. The academic research community and industry have used numerical simulation for a long time in order to analyze, design and optimize complex wireless systems. On the other hand, there are the fundamental issues of credibility and reproducibility when the conclusions are only based on simulations results. Hence, we have been carried out efforts to validate our simulation results using both analytical expressions and comparisons with results from the open literature.

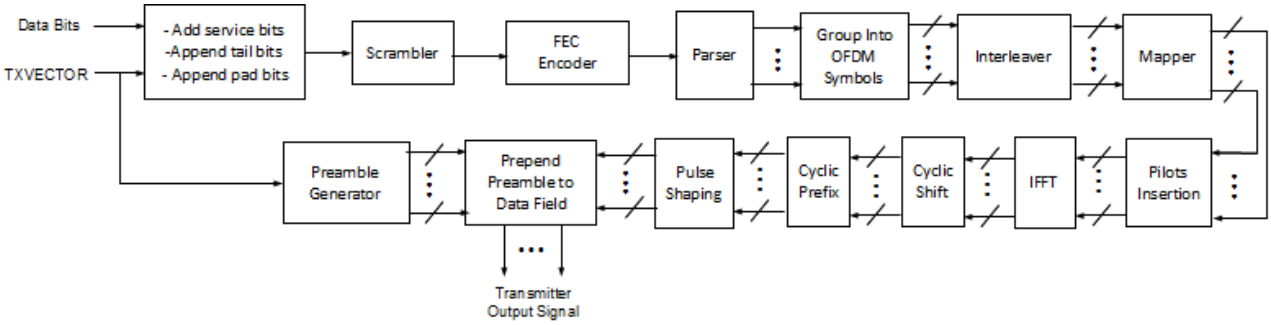

Fig. 2. Transmitter block diagram.

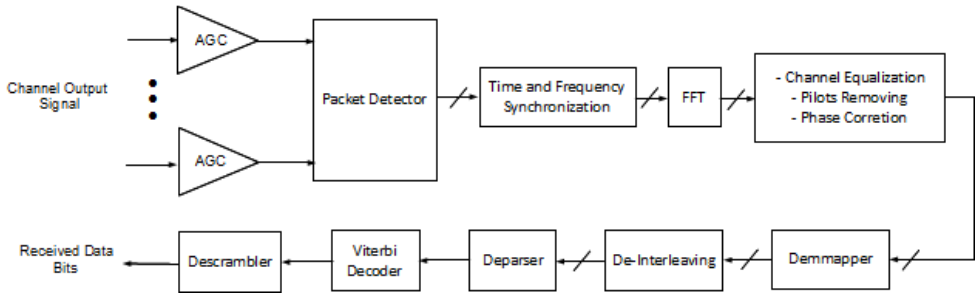

Fig. 3. Receiver block diagram.

To accomplish this challenging task, we have proceeded as follows. First, in subsection III-A, we define precisely the reference parameters used to assess the system performance. This step is of fundamental importance since we have been noticing that not all published papers have done it precisely, making extremely difficult to establish comparisons and reproduce the shown results. In the following, in subsection III-B, we develop first order analytical expressions to relevant performance metrics, such as bit error rate (BER) and packet error rate (PER). Finally, in section IV, we perform a consistent comparison between simulation and analytical results.

A. Reference Parameters

In this subsection, we derive a relation between the available energy per bit E_b and transmitted OFDM symbol energy E_{OFDM}. This is the energy available to distribute along the whole symbol, including the multiple transmitting antennas and signaling overheads. Therefore,

$$E_b = E_{OFDM}\left(\frac{1}{N_{TX}}\right)\left(\frac{\mathrm{N_{FFT}}}{\mathrm{N_{FFT}+N_{CP}}}\right)\left(\frac{N_{data}}{N_{data}+N_{pilot}}\right)\left(\frac{1}{N_{data}\,N_{BPSCS}\,R}\right), \quad (1)$$

where N_{TX} is the number of transmitting antennas. Assuming a bandwidth of 20 MHz, we have: *(i)* FFT length ($\mathrm{N_{FFT}}$) of 64 samples; *(ii)* CP length ($\mathrm{N_{CP}}$) of 16 samples; *(iii)* number of data subcarrier ($\mathrm{N_{data}}$) equals to 52; *(iv)* number of pilot subcarriers ($\mathrm{N_{pilot}}$) equals to 4. The first term divides the energy among the transmitting antennas. The second one accounts for the reduction in the available energy due to the CP. The third term models the reduction of the net energy due to the pilot symbols that do not transport information. Finally, the last term shows how that the remaining net energy is divided among the bits of each transported symbol. Note that the code rate R is smaller than one, increasing the necessary energy per bit at the FEC encoder input.

Based on the derived relation between E_{OFDM} and E_b, then we are able to determine a relation between the SNR (Signal-to-Noise Ratio) and $\frac{E_b}{N_0}$ (SNR per bit or the ratio of energy per bit to one-side noise spectral density N_0). The SNR is defined as the ratio of signal power to noise power at the input of each receiver antenna:

$$SNR = \frac{P_{signal}}{P_{noise}}. \quad (2)$$

The version of the simulator used in this paper implements a discrete baseband model. Hence, the signal power per stream is the energy (variance) per time sample in each stream. It is given by

$$P_{signal} = \frac{E_{OFDM}}{\mathrm{N_{tx}}}\,\frac{1}{(N_{CP}+N_{FFT})}, \quad (3)$$

i.e., the power is the OFDM symbol energy per stream divided by number of samples of each OFDM symbol with CP.

The one side spectral density N_o is the variance per complex sample of the circularly symmetric Gaussian random variable (rv). Therefore, using (1) and (3) in (2), the SNR can be modeled as

$$SNR = \frac{E_b}{N_0}\left(\frac{\mathrm{N_{FFT}+N_{CP}}}{\mathrm{N_{FFT}}}\right)\left(\frac{N_{data}+N_{pilot}}{N_{FFT}+N_{CP}}\right)(N_{BPSCS}\,R), \quad (4)$$

that can be rewritten as

$$SNR = \frac{E_b}{N_0}\left(\frac{N_{data}+N_{pilot}}{N_{FFT}}\right)(N_{BPSCS}\,R). \quad (5)$$

B. Analytical Results for AWGN MIMO Channels

The simulation of AWGN channels, besides of its intrinsic importance to determine fundamental parameters (such as receiver sensitivity and implementation margins), allows validating the signal processing flow in the transmitter (cf. Fig. 2) and receiver (cf. Fig. 3). The AWGN model was proposed as comparison criteria for the PHY layer performance of the submitted proposals during the 802.11n standardization process [6].

The MIMO matrix H (cf. Eq. 6) is obtained taking the first N_{rx} x N_{tx} elements from the Fourier matrix with dimension $N = \max(N_{rx}, N_{tx})$, where $W = \exp(-j2\pi/N)$ [6]. Notice that the rows and columns of the Fourier matrix are orthogonal and, consequently, the implementation of a decorrelator receiver allows decoupling the transmitted streams without noise enhancement.

$$H_N = \begin{bmatrix} 1 & 1 & 1 & \cdots & 1 \\ 1 & W^1 & W^2 & \cdots & W^{(N-1)} \\ 1 & W^2 & W^4 & \cdots & W^{2(N-1)} \\ \vdots & \vdots & \vdots & \ddots & \vdots \\ 1 & W^{(N-1)} & W^{(N-1)2} & \cdots & W^{(N-1)^2} \end{bmatrix}. \quad (6)$$

The analytical equations developed in this section models the probability of error at Viterbi decoder output when it is used hard-decision decoding. The probability of incorrectly selecting a path when the Hamming distance d is even and odd is given by (7) and (8), respectively [7]. The BER at the hard decision demodulator output for the mth MCS is denoted by ρ_m. The SNR per coded bit at the Viterbi decoder input is denoted by γ_c.

$$P_{\mathrm{d}}(\gamma_c, m) = \frac{1}{2}\binom{d}{d/2}\rho_m^{d/2}(1-\rho_m)^{d/2} + \sum_{k=\frac{d}{2}+1}^{d}\rho_m^k(1-\rho_m)^{d-k}. \quad (7)$$

$$P_d(\gamma_c, m) = \sum_{k=\frac{d+1}{2}}^{d}\binom{d}{k}\rho_m^k(1-\rho_m)^{d-k}. \quad (8)$$

The basic 802.11n BCC has code rate ½ and polynomial generators given by $g_0 = (133)_8$ and $g_1 = (171)_8$. The union bound for the probability of decoding error is given by (9) [7]. Higher coding rates are obtained by bit puncturing the original ½ BCC. For the BCC with code rate ¾, the union bound is given by (10).

$$P_{\mathrm{e}}(\gamma_c, m) = 11P_{10}(\gamma_c, m) + 38P_{12}(\gamma_c, m) + 193P_{14}(\gamma_c, m) + \cdots. \quad (9)$$

$$P_e(\gamma_c, m) = 8P_5(\gamma_c, m) + 31P_6(\gamma_c, m) + 160P_7(\gamma_c, m) + \cdots. \quad (10)$$

When the errors inside of the decoder are interdependent, then an upper bound for the packet error rate (PER) considering a frame with l *octets* is given by [8,7]

$$PER(\mathrm{l}, \gamma_c, m) < 1 - [1 - P_e(\gamma_c, m)]^{8l}. \quad (11)$$

C. Analytical Results for Underspread Fading Channels

In this section, it is assumed a slow fading channel (i.e., the coherence time is significant lower than the delay requirements of

the application). Hence, the errors inside of the decoder are interdependent, and an upper bound for the PER assuming a frame with *l* octects is given by

$$PER(l,\gamma_c) \le 1 - \int_{\gamma_{inf}}^{\infty} [1 - P_e(\gamma_c)]^{8l} p(\gamma_c) d\gamma_c, \quad (12)$$

where the lower limit of the definite integral is chosen so that

$$[1 - P_e(\gamma_c)]^{8l} \le 1 \ \ for\ \gamma_c \ge \gamma_{inf}. \quad (13)$$

The frequency diversity due to the joint effects of channel and interleaving creates L_d diversity branches, where the diversity order depends on the root mean square (RMS) of the multipath channel power delay profile (PDP).

Considering a Nakagami-m fading channel with L_d independent diversity branches with the same average received power, then the probability density function (pdf) of the SNR per coded bit at the Vitrbi decoder input is Gamma kind [7]:

$$p(\gamma_c) = \frac{1}{\Gamma(L_d\, m_n)} \left(\frac{m_n}{\overline{\gamma_c}}\right)^{L_d\, m_n} (\gamma_c)^{L_d\, m_n - 1}\, exp\left(-\frac{m_n \gamma_c}{\overline{\gamma_c}}\right) \ \text{if}\ \gamma_c > 0, m_n \ge 0.5, \quad (14)$$

where Γ(.) denotes the gamma function, m_n is the Nakagami-m fading figure (e.g., $m_n=1$ for Rayleigh). Using (5), then the average SNR per coded bit at the Viterbi decoder is given by

$$\overline{\gamma_c} = \frac{E_b R}{N_0} = \text{SNR}\left(\frac{N_{FFT}}{N_{data}+N_{pilot}}\right)\frac{1}{N_{BPSCS}}. \quad (15)$$

It is postulated that there is not inter-stream interference in our first-order analytical model. Assuming hard decision demodulation, then the instantaneous raw BER for BPSK and quaternary PSK (QPSK) for the *k*th OFDM subcarrier at the Viterbi decoder input is given by (16) and (17), respectively, where *Q(x)* is the complementary Gaussian cumulative distribution function. Note that it is used (5) with $N_{BPSC}=1$ and $N_{BPSC}=2$ for BPSK and QPSK, respectively.

$$\rho_{BPSK} = Q\left(\sqrt{\frac{2E_bR}{N_0}}\right) = Q\left(\sqrt{2\,\text{SNR}\left(\frac{N_{FFT}}{N_{data}+N_{pilot}}\right)}\right). \quad (16)$$

$$\rho_{QPSK} = Q\left(\sqrt{\frac{2E_bR}{N_0}}\right) = Q\left(\sqrt{\text{SNR}\left(\frac{N_{FFT}}{N_{data}+N_{pilot}}\right)}\right). \quad (17)$$

For rectangular M-ary quadrature amplitude modulation (M-QAM), the instantaneous raw BER for the *k*th OFDM subcarrier at the Viterbi decoder input is obtained using (5) in the BER expression derived in [9], resulting in

$$\rho_{QAM} = \frac{\sqrt{M}-1}{\sqrt{M}\, log_2(\sqrt{M})} erfc\left(\sqrt{\frac{2\text{N}_{\text{BPSC}}\text{R}}{M-1}\frac{E_b}{N_0}}\right) + \frac{\sqrt{M}-2}{\sqrt{M}\, log_2(\sqrt{M})} erfc\left(\sqrt{\frac{3\text{N}_{\text{BPSC}}\text{R}}{2(M-1)}\frac{E_b}{N_0}}\right), \quad (18)$$

where *erfc(z)* is the complementary error function.

IV. Numerical and Analytical Results

Hereafter, it is assumed perfect time and frequency synchronization. The reader is referenced to [2] to obtain analytical and numerical results on the time and frequency synchronization in IEEE 802.11n networks.

A. AWGN MIMO Channel

In this subsection, it is used the N x N MIMO channel matrix defined in (6). Assuming perfect channel estimation, the transmitter and receiver antennas can be decoupled, and, therefore, the PER is only function of SNR per stream (cf. Eq. 5), i.e., independent of the number of antennas.

Fig. 4 shows the PER over an AWGN channel as a function of SNR for BPSK, QPSK and 16-QAM using BCC with code rate ½. Fig. 5 shows similar results, except that now it used QPSK, 16- and 64-QAM using BCC with code rate ¾. It is shown results for soft and hard-decision Viterbi decoding. The packet has a payload of 4096 bytes. The Viterbi decoder has a trace back length (TBL) of 35 for the code rate ½. The TBL is increase to 50 when it is used bit puncturing to avoid performance degradation.

Figures 4 and 5 also show the analytical upper bounds for hard decision Viterbi decoder, which were obtained using the equations developed in subsection III-B. These equations must be parameterized using adequate values of N_{BPSCS} for each MCS (cf. Table I). Observe that the results obtained for BPSK and QPSK signaling are different since the results are plotted as a function of SNR and not as function of SNR per bit E_b/N_0. Therefore, the BPSK has half of SNR since it uses only the in-phase dimension (see 16 and 17). It is observed an excellent agreement between the theoretical lower bounds and simulation results for hard-decision decoding. As expected, the soft-decision decoding allows a decoding gain greater than *2 dB* in relation to the hard decision decoding. Comparing these results with the ones presented in the excellent *Perahia's and Stacey's* book [4], where it is shown *only simulation results* for the PER over AWGN channels using soft-decision Viterbi decoding, we can also verify a good agreement among them. We conclude, based on the shown analytical and simulation results, that the complex state machine that models the signal flow in the IEEE 802.11n transmitter and receiver is validated, i.e., a fundamental issue for credibility.

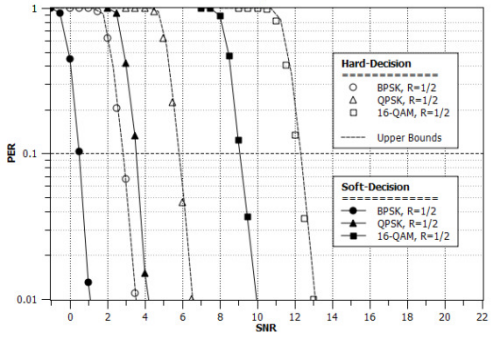

Fig. 4. PER as a function of SNR over an AWGN channel for BPSK, QPSK and 16-QAM using BCC with code rate ½.

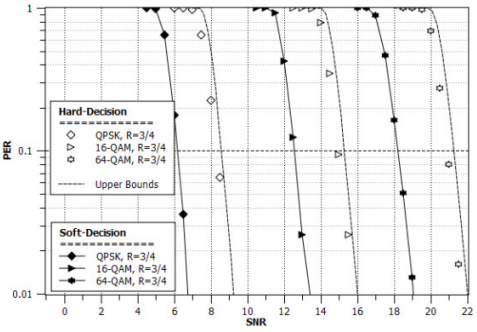

Fig. 5. PER as a function of SNR over an AWGN channel for QPSK, 16-QAM and 64-QAM using BCC with code rate ¾.

B. TGn MIMO Channel A

The TGn MIMO channel models, suited for indoor MIMO simulations, were developed during the 802.11n standardization process [4, p. 35, 9]. There are five, labeled from A to F, spatial correlated MIMO channel models with PDP based on the cluster model. The *TGn A model* is flat fading Rayleigh channel, used for stressing the system performance due to lack of frequency diversity [4].

Fig. 6 shows the PER as a function of SNR per stream assuming perfect channel estimation. It is shown results for BPSK and 16-QAM. It is assumed a ZF receiver and soft-decision Viterbi decoding. The best performance is obtained with one antenna due to the absence of inter-stream interference. Note that it is not possible to guarantee orthogonality among the spatial streams, and,

therefore, there is a performance degradation due to the inter-stream interference.

Fig. 7 shows the PER for BPSK and 16-QAM as a function of SNR per stream over a TGn A channel model. It is implemented a MMSE receiver with a realistic channel estimation scheme. Again the best results are obtained with just one antenna. It is observed an excellent agreement between analytical and simulation for hard-decision Viterbi decoding. The analytical results for the PER are obtained using $L_d=1$ in (14), i.e., there is no frequency diversity since the fading is non-selective.

Comparing figures 6 and 7, we can see a performance improvement for BPSK signaling when it is implemented the MMSE receiver due to the reduction of inter-stream interference (e.g., for the MCS24 a PER of 1% is obtained with a SNR of 22 dB with ZF receiver and 16 dB with MMSE receiver). However, we can verify that the MMSE receiver does not allow any performance improvement for the 16-QAM signaling as the number of antennas increase. Note that in this case of high cardinality modulation, the self-interference must be mitigated with MMSE coupled with successive interference cancelation.

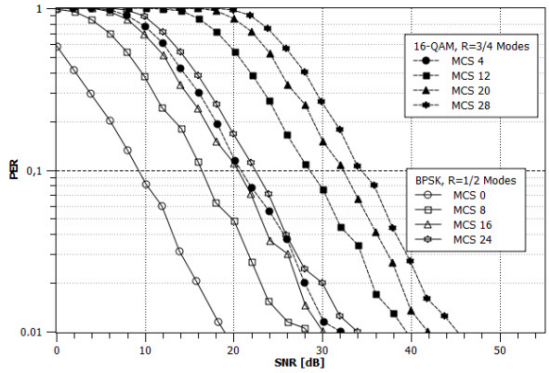

Fig. 6. PER as a function of SNR over a TGn A channel for BPSK and 16-QAM with perfect channel estimation and soft-decision Viterbi decoding.

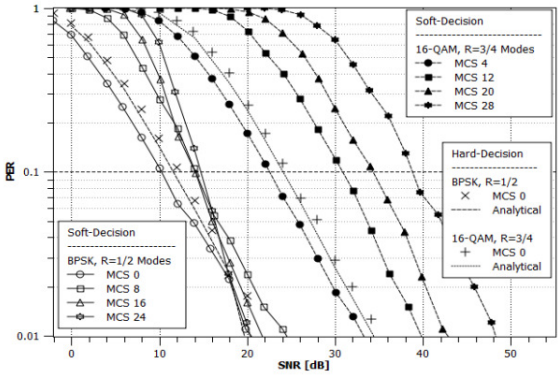

Fig. 7. PER as a function of SNR over a TGn A channel for BPSK and 16-QAM using a MMSE receiver with soft and hard-decision Viterbi decoding.

C. TGn MIMO Channel F

The *TGn channel model F* is used to simulate large indoor spaces [4, p. 36]. It has a RMS delay spread of *150 ns*, and the coherence bandwidth can be approximated by

$$W_c = \frac{1}{2T_d} = \frac{1}{2\cdot(150\times10^{-9})} = 3.33 \times 10^6 \ Hz. \quad (19)$$

Therefore, for a bandwidth of *W= 20 MHz* the diversity gain is given by

$$L_d = \frac{W}{W_c} = \frac{20\times10^6}{3.33\times10^6} \cong 6. \quad (20)$$

Fig. 8 shows results for BPSK using BCC with code rate *1/2* over TGn A and TGn F channels. The packet length is *1024 bytes*. It is assumed a MMSE receiver with soft-decision Viterbi decoding and a realistic channel estimation procedure The TGn F channel presents frequency diversity (cf. 20). Consequently, it is observed a significant improvement on the PER performance in relation to the TGn A channel. However, the TGn F channel model is challenging since it demands better channel estimation algorithms and more advanced receivers (e.g., MMSE with successive cancellation techniques) due to the high conditional number of the equivalent MIMO channel matrix that increases the challenging of separating the spatial streams as the number of antennas increase. Note the results in Fig. 8 corroborate this reasoning, since the performance is presents a strong dependence with the number of streams for the TGn F channel model

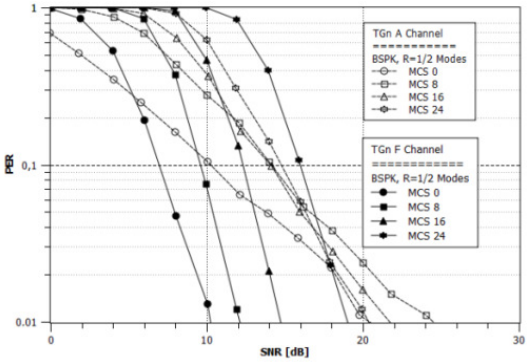

Fig. 8. PER as a function of SNR over TGn A and F channels for BPSK signaling using a MMSE receiver with soft decision Viterbi decoding.

V. FINAL REMARKS

In this paper, we first jointly described the IEEE 802.11n PHY layer and a computational simulator developed in Matlab and C++. Second, we derived a relation between SNR and SNR per bit using the 802.11n PHY layer parameters. Third, we developed analytical expressions to assess the PER over AWGN and Nakagami-m fading channels. Finally, these expressions were used to validate a consistent computational and analytical framework for the IEEE PHY 802.11n standard, comparing simulation and numerical results for AWGN, TGn A and TGn F channel models.

REFERENCES

[1] Wireless LAN Medium Access Control (MAC) and Physical Layer (PHY) Specifications, Amendment 5: Enhancement for Higher Throughput. IEEE Std 802.11n-2009, 2009.

[2] A. M. Câmara and R. P. F. Hoefel , "On the performance of IEEE 802.11n cyclic shift diversity scheme for 802.11a/g legacy compatibility", in Vehicular Technology Conference 2011 Spring, VTC 2011-Spring, Budapeste, 2011.

[3] *Wireless LAN Medium Access Control (MAC) and Physical Layer (PHY) Specifications, High-speed Physical Layer in the 5 GHz Band.* IEEE Std 802.11a-1999, 1999.

[4] E. Perahia and R. Stacey, Next Generation Wireless LANS. New York, USA: Cambridge University Press, 2008.

[5] F. Tosato and P. Bisagli, "Simplified soft-output demapper for binary interleaved COFDM with applications to HIPERLAN/2, " IEEE International Conference on Communications 2002, 2002.

[6] B. A. Bjerke, et al, *TGn Comparison Criteria – Proposal for CC59.* IEEE 802.11-04/176r0, 2004.

[7] R. P. F. Hoefel. "Goodput and delay cross-layer analysis of IEEE 802.11a networks over block fading channels," Proc. of IEEE Consumer Comm. Networking Conf. 2006, Las Vegas. 2006.

[8] M. B. Pursley and D. J. Taipale. "Error probabilities for spread-spectrum packet radio with convolutional codes and Viterbi decoding," IEEE Trans. Commun., vol. 35, n. 1, p. 1-12, 1987.

[9] L. Yang and L. Hanzo, "A recursive qlgorithm for the error probability evaluation of *M*-QAM," IEEE Communications Letters, vol. 4, n. 10, p. 304-306, October 2000.